

# Influence of Air on the Bouncing Dynamics of Shallow Vibrated Granular Beds: Kroll's Model Predictions

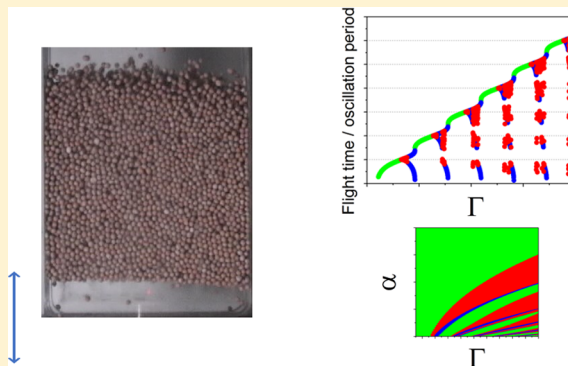
Bruno V. Guerrero,<sup>†,‡</sup> Vladimir I. Idler,<sup>¶</sup> and Iván J. Sánchez<sup>\*,†,§</sup>

<sup>†</sup>Centro de Física, Instituto Venezolano de Investigaciones Científicas (IVIC), AP 20632, Caracas 1020-A, Venezuela

<sup>¶</sup>Departamento de Física, Universidad Simón Bolívar, Caracas 1080-A, Venezuela

**S** Supporting Information

**ABSTRACT:** In the present work, we explore the modification of the periodicity of the motion of shallow granular columns in the framework of Kroll's one-dimensional model for the motion of a vibrated bed. Within the model, bed dynamics depend on two parameters, the dimensionless maximum acceleration,  $\Gamma$ , and a dissipative parameter,  $\alpha$ , depending on air viscosity, grain density, bed static porosity, oscillation frequency and grain diameter. We show how the bifurcation diagram for the flight time of the bed as a function of  $\Gamma$  changes with  $\alpha$ . For  $\alpha = 0$ , Kroll's prediction equals that of the inelastic bouncing ball model. When  $\alpha$  is increased, bifurcations shift to higher  $\Gamma$  up to a point where not even a single bifurcation is predicted in a range of  $\Gamma$  where an inelastic bouncing ball displays several bifurcations. We also illustrate how the flight time reduces nonlinearly with increasing  $\alpha$  in a monotonic way. We introduce isoperiodic maps to illustrate regions of single, double, or more periodicities in the phase space. We also show and discuss the dependence of the flight time on the parameters entering the definition of  $\alpha$  within ranges of those parameters that have been explored in the literature. Grain diameter, grain density and vibration frequency are the most determinant.



## INTRODUCTION

Vibrated granular beds are commonly used in industry for operations like size separation, milling, and transport. In many cases, the interest for vibrated beds responds to the widespread use of vibrofluidized beds, where mechanical excitation due to vibrations is added to the fluidizing effect of a passing fluid. However, the case of pure vibrations (without aeration) is still complex and encompasses many interesting transport phenomena. Theoretical modeling of vibrated beds has followed several, sometimes combined, paths from the description of the mechanical response of a vibrated bed to the study of heat transfer capabilities and the modeling of the flight dynamics of the bed. The latter is of special interest because it can shed light on the time response of shallow beds, where the column behaves as a solid block. Adequately tuning this time response may enhance the result of bulk solids management operations like vibratory transport,<sup>1–7</sup> vibrated bed dryers<sup>8–11</sup> and vibrated bed reactors.<sup>12,13</sup>

The simplest approximation to a vibrated bed is the well-known inelastic bouncing ball model (IBBM).<sup>14–16</sup> The IBBM describes the motion of a single point mass, bouncing on a sinusoidally driven plate, considering completely inelastic collisions with the plate. Its application to vibrated beds is widespread.<sup>2,3,17–21</sup> One of the main features of the dynamics of the IBBM is the period doubling scenario<sup>22</sup> observed for the dependence of bouncing ball's flight time on the maximum dimensionless acceleration  $\Gamma$ . Period doubling is a common

dynamical feature of both a single mass and vibrated particle beds, at least in a regime of shallow, dense beds: a single vertical column of grains<sup>23</sup> and two-dimensional<sup>24</sup> and three-dimensional beds<sup>20,25–27</sup> display a period doubling scenario similar to the IBBM. In recent years, several studies have explored options for including dissipation in the bouncing motion of a single object on a vibrating plate, for example, allowing the vibrating plate to be able to bend<sup>28</sup> or considering either a spring,<sup>29</sup> a liquid droplet,<sup>30</sup> or a sand filled ball<sup>31</sup> instead of a single point mass and considering air drag.<sup>32,33</sup>

The main issue with using IBBM for vibrated beds is that the model only considers parameters describing the forcing, and there is no way to compare between beds of different characteristics.

One of the main factors affecting the motion of a vibrated granular bed is its interaction with interstitial air (having critical importance in segregation<sup>34–37</sup> and transport phenomena<sup>6,38–40</sup>). This has inspired a couple of recent experimental studies on air effects on the period bifurcation of vibrated beds: the works of Pastor et al.<sup>41</sup> and Han et al.<sup>42</sup> Those authors compared their results with theoretical predictions from Kroll's model for a vibrated bed,<sup>43,44</sup> obtaining a good agreement

**Received:** December 26, 2015

**Revised:** April 13, 2016

**Accepted:** April 15, 2016

**Published:** April 15, 2016

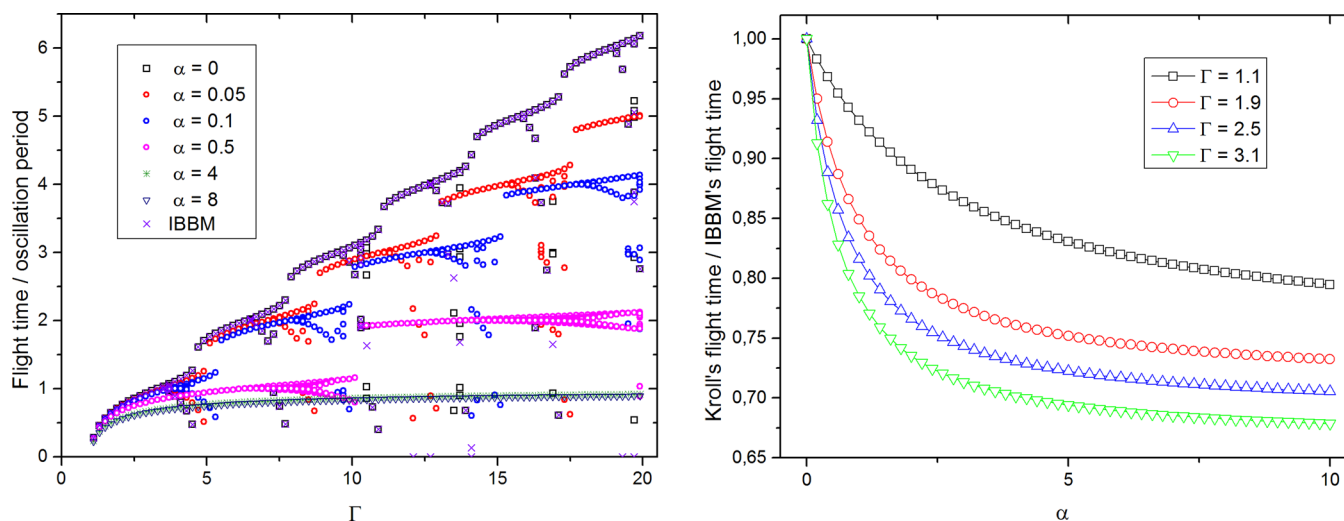


**Figure 1.** (left) Bifurcation diagram for different  $\alpha$  values compared with that of the IBBM. (right) Dependence of flight time with  $\alpha$  at fixed  $\Gamma$ . Only a couple of low  $\Gamma$  cases with a single flight time are shown to illustrate the trend.

between experimental and theoretical flight times, at least for their specific parameter configuration.

Following the interest aroused by the experimental studies of refs 41 and 42 and looking forward to achieve a theoretical understanding of the bouncing dynamics of a vibrated bed with a model that considers experimental characteristics of vibrated beds used for industrial application design, in this article, we explore Kroll's model predictions over a wide range of parameters, inspired by configurations used in literature studies as well as in industrial applications. Still nowadays, apparently simple machinery like vibratory separators represent a challenge for resizing and rescaling, and manufacturers often rely on past experience.<sup>45</sup> In the field, specially when on a budget, changing a motor or a shaft, the grain size, or the interstitial fluid (to avoid explosion hazards or to improve drying) of an already working process is a tough question. Handbooks provide limited information about parametric response of vibrated beds.<sup>46</sup> The revisit presented in the following pages aims to provide a theoretical framework within selected parameter ranges, information that was implicit in Kroll's model bed equation, but has not been explored in the past.

## OVERVIEW OF KROLL'S MODEL

Kroll's model uses a one-dimensional equation to describe the motion of a porous piston, assuming the piston moves through an incompressible fluid and using Darcy's law to describe fluid flow through the piston. An analytic solution for the position of the bed and for the pressure drop across it can be obtained. Kroll's model represents the starting point for incorporating other processes like bed expansion<sup>47</sup> or aerated vibrated beds.<sup>48</sup> The granular bed is assumed to behave as a solid porous block, moving on a plate oscillating along the vertical direction according to  $z(t) = A \sin(\omega t)$ , with  $A$  being the amplitude,  $f = \omega/(2\pi)$  being the frequency of oscillation, and  $t$  being time. The maximum dimensionless acceleration is  $\Gamma = A\omega^2/g$ , with  $g$  being the acceleration of gravity. Take off occurs at a time  $t_0 = \frac{1}{\omega} \arcsin(1/\Gamma)$ . During the bed's flight, a gap of size  $s$  separates it from the plate, and the equation of motion is given by

$$\ddot{s}(t) - \frac{B}{m}(\Delta P) = -\dot{z}(t) - g \quad (1)$$

where  $\Delta P$  is the pressure difference between the top and bottom of the bed,  $B$  is the cross sectional area of the container,  $m$  is the mass of the bed, and dots indicate derivatives with respect to time. The bed is assumed to have a bulk density,  $\rho_m = (1 - \phi)\rho_g$  with  $\rho_g$  being the density of a single grain and  $\phi$  being the porosity of the bed (assuming that fluid density is much lower than  $\rho_g$ ). Relating the volumetric flow rate  $Q$  through the bed with the mass of fluid contained within the gap,  $G = \rho_f B s$  (fluid density,  $\rho_f$  is constant because the fluid is assumed to be incompressible), it is possible to deduce that  $Q = B\dot{s}$ . Using this last relation for  $Q$  and Darcy's law,<sup>49</sup> one obtains the following equation<sup>36,43</sup> for  $\dot{s}$ :

$$\dot{s}(t) = k \frac{\Delta P}{h} \quad (2)$$

where  $h$  is the bed's height,  $k \equiv K/\eta$  is the relative permeability,  $\eta$  is the dynamic viscosity, and  $K$  is the intrinsic permeability (depending only on geometrical properties of the solid matrix<sup>50</sup>). For a random pack of spheres under laminar flow conditions, the Carman Kozeny equation holds for the permeability,<sup>50,51</sup> given by

$$K = \frac{d^2}{180} \frac{\phi^3}{(1 - \phi)^2} \quad (3)$$

where  $d$  is the diameter of a single grain. Using eqs 3 and 2 in eq 1, one obtains the final equation for  $\dot{s}$ , describing the dynamics of the granular column:

$$\ddot{s}(t) + \dot{s}(t) \frac{Bh\eta}{mK} = g[\Gamma \sin[\omega(t + t_0)] - 1] \quad (4)$$

Equation 4 can be written in terms of two dimensionless variables,  $s'(\psi) \equiv s(t)/A$  and  $\psi \equiv \omega t$ :

$$\ddot{s}'(\psi) + \alpha \dot{s}'(\psi) = \frac{1}{\Gamma} [\Gamma \sin[\psi + \psi_0] - 1] \quad (5)$$

where  $\psi_0 = \arcsin(\Gamma^{-1})$  is the dimensionless take off time and  $\alpha$  is a dimensionless dissipative parameter given by

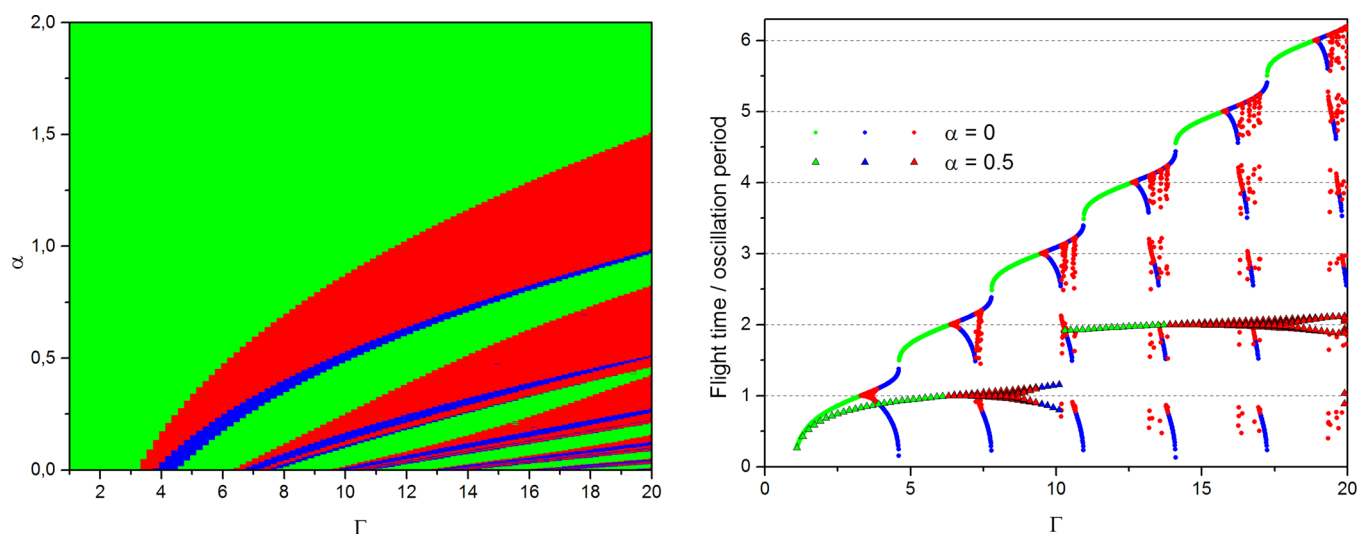


**Figure 2.** (left) Isoperiodic map  $\alpha$ – $\Gamma$  obtained from numerical determination of the flight time of a vibrated granular bed, using Kroll’s model. Green, blue, and red color indicate regions with one, two, and three or more periodic flights. (right) Illustration of the color code used for the isoperiodic map at the left, for the bifurcation diagram of the IBBM (case with  $\alpha = 0$  corresponding to the bottom horizontal line of the isomap at the left) and for the case with  $\alpha = 0.5$ .

$$\alpha = \frac{Bh\eta}{\omega m K} = \frac{\eta}{\omega K \rho_m} = \frac{180\eta(1-\phi)}{d^2\omega\rho_g\phi^3} \quad (6)$$

Equation 5 shows how two dimensionless parameters dictate the dynamics of the bed:  $\Gamma$ , which characterizes the energy injection and  $\alpha$ . This parameter  $\alpha$  is the frictional factor controlling energy dissipation via air drag,<sup>36,42</sup> closely related to coefficients previously defined in air-damped bouncing ball studies.<sup>32,33</sup> Also  $1/\alpha$  could be interpreted as the characteristic time needed for the column to reach a regime where its motion is governed by the viscosity of the fluid.<sup>52</sup> In the context of vibrated beds moving in air,  $\alpha$  has the significance of other dimensionless numbers such as Bagnold’s number used to characterize flow regimes of liquid–particle suspensions<sup>53</sup> or Reynolds and Froude numbers used in fluid mechanics. Physically speaking, the parameter  $\alpha = \eta/(\omega K \rho_m)$  is a ratio of viscosity to the momentum of the bed.

## OVERALL DEPENDENCE OF BED’S FLIGHT DYNAMICS ON DISSIPATIVE PARAMETER $\alpha$

Figure 1 shows the bifurcation diagram for different values of the dissipative parameter  $\alpha$ . The IBBM prediction is included as a reference and can be seen to match exactly the case with  $\alpha = 0$  (essentially Kroll’s model reduces to the IBBM in the absence of dissipation). As the value of  $\alpha$  is increased the main effect is a drift from the IBBM behavior that is more pronounced at larger  $\Gamma$ . See, for example, the curve for  $\alpha = 0.05$ : it shows only four bifurcations, while the IBBM shows six bifurcations within the same range in  $\Gamma$ . For cases with  $\alpha \geq 4$  where for the range of  $\Gamma$  explored, there is not even a single bifurcation. Deviation from the IBBM behavior is more pronounced at larger  $\Gamma$  for a fixed  $\alpha$ . See, for example, the curve for  $\alpha = 0.05$ : at  $\Gamma \approx 4$ , there is not a significant deviation from the IBBM, but for  $\Gamma \approx 18$ , the difference is on the order of 20%. Larger  $\alpha$  values display a further departure of Kroll’s model with respect to the IBBM. The departure can be appreciated in more detail if one takes a look at Figure Sequence S1 of the Supporting Information.

For low values of  $\Gamma$ , before any bifurcation takes place, it is possible to observe a smooth functional dependence of the

flight time with  $\alpha$  at fixed  $\Gamma$ . Figure 1 (right) illustrates this functional dependence, resulting in a monotonically decreasing function. Although it may resemble an exponential or a power law decay, we tested both fits and obtained merely fair agreement. This plot gives us an idea of how important is the deviation from the IBBM behavior when  $\alpha$  is increased with fixed  $\Gamma$ . Within the range of  $\alpha$  explored, we can see that a reduction of the order of 30% of the flight time with respect to the flight time predicted by the IBBM can be obtained. Again a more pronounced deviation from the IBBM is observed at larger  $\Gamma$ .

An alternative way to look at the information from the bifurcation plots is to look at the corresponding “isoperiodic maps”.<sup>54</sup> For example, take a look at the  $\alpha$ – $\Gamma$  isoperiodic map shown in Figure 2. Different colors indicate the periodicity according to the definition of Gilet et al.:<sup>22</sup> “a period- $n$  motion involves  $n$  different flights”. The map illustrates zones in the  $\alpha$ – $\Gamma$  parameter space having a single flight (displayed in green), two flights (displayed in blue), and three or more flights (displayed in red). Each horizontal line from the isoperiodic map is obtained from a bifurcation plot like those illustrated in Figure 1. Two bifurcation plots for  $\alpha = 0$  and  $\alpha = 0.5$  are shown at the right side of Figure 2 to explain the color code used.

The map of Figure 2 is basically a modified and simplified version of the map presented by Han et al.<sup>33</sup> in Figure 5 of their work. It is modified since their calculation is based on a modification of the IBBM model including an air damping factor without including parameters related to a vibrated granular bed; besides we explore a smaller  $\Gamma$  range and a larger  $\alpha$  range. It is simplified, since we do not pay attention to the chaotic behavior (any chaotic zone will be included in a red zone). An important remark in our case is the fact that we do not look for the asymptotic behavior, as has been usually done in previous works.<sup>32,35,41</sup> We took a different approach because industrial applications may include residence times that are small compared with asymptotic times of several thousands of oscillation cycles used previously.

The map of Figure 2 could be an important reference when dealing with the design of vibrated bed process machinery. For example, during vibratory conveying, it may be important to

Table 1. List of Estimated  $\alpha$  Values or Ranges Used in Some Representative Previous Experimental Studies on Vibrated Beds<sup>a</sup>

ref	$\sim d$ (mm)	$f$ (Hz)	grain	interstitial gas	$\Gamma$	$\alpha$
2	1–1.5	40–70	glass, calcite	air	2–3.5	0.02–0.08
25	0.63–0.8	10–100	glass, salt	air–vacuum	0–13	0–0.91
55	0.099–0.332	30–80	glass, alumina, sand	air	3–8	0.35–10.5
26	0.15–0.018	10–110	bronze	vacuum	1–8.5	0
56	0.2–2	7.78	glass	propane–helium	1.3	0.04–4.40
20	1.28–3	15–40	glass	air	0–8	0.01–0.13
19	2.85	10	glass	air	0.5–2.5	0.04
57	0.088–0.707	25	alumina	air	2–7	0.17–11.01
27	0.5–1	30–70	stainless steel	air	1–17.5	0.02–0.14
41	0.5	110	glass	air–vacuum	1–6	0–0.11
42	0.35–1	40–80	stainless steel	air–vacuum	1–16	0–0.22
52	0.465	15–50	stainless steel	air	1–4	0.10–0.32

<sup>a</sup>Here, it was assumed:  $\rho_{\text{glass}} = 2500 \text{ kg/m}^3$ ,  $\rho_{\text{alumina}} = 3650 \text{ kg/m}^3$ ,  $\rho_{\text{stainless-steel}} = 7400 \text{ kg/m}^3$ ;  $\eta_{\text{air}} = 1.98 \times 10^{-5} \text{ Pa}\cdot\text{s}$ ,  $\eta_{\text{vacuum}} = 0 \text{ Pa}\cdot\text{s}$ ,  $\eta_{\text{propane}} = 8.71 \times 10^{-6} \text{ Pa}\cdot\text{s}$ ,  $\eta_{\text{helium}} = 2.13 \times 10^{-5} \text{ Pa}\cdot\text{s}$ ;  $\phi = 0.36$  (random close packing).

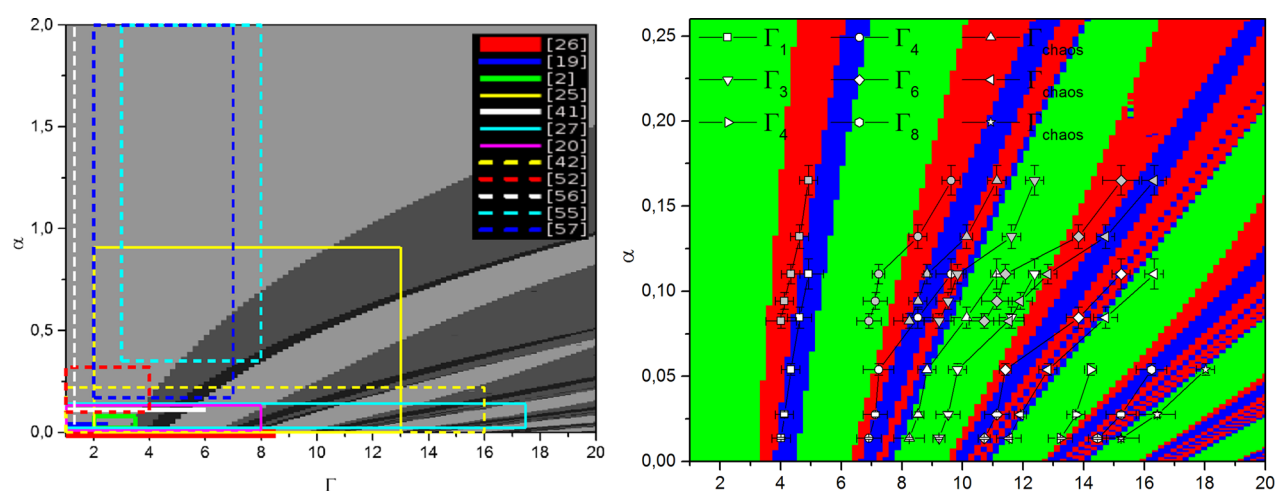


**Figure 3.** (left) Isoperiodic map  $\alpha$ – $\Gamma$  with rectangles or lines indicating the range of parameters explored in some literature studies. (right) Zoom of the  $\alpha$ – $\Gamma$  isoperiodic map showing two data sets from experiments performed by Han et al.<sup>42</sup> who used stainless steel spheres of different sizes. White filled symbols correspond to the data set of Figure 4 from ref 42 taken at different grain diameters at 60 Hz in air. Gray filled symbols correspond to the data set of Figure 5 from ref 42 taken at different frequencies for a fixed grain diameter of 0.35 mm in air. Static bed porosity was assumed to be equal to 0.38, and air viscosity was taken to be  $2 \times 10^{-5} \text{ Pa}\cdot\text{s}$ . Horizontal error bars are taken from experimental data. Vertical error bars are propagated from experimental uncertainties reported by Han et al., assuming a 0.1% uncertainty for the frequency, 1% for the viscosity, and 5% for the static bed porosity.

ensure a combination of parameters giving a response of the bed with the same periodicity of the forcing. A double or higher period scenario may represent a waste of energy since if one of the flights is the optimal then the rest of flights are not because the granular material does not reach the same dilation or the same flight time. Of course there may be situations where multiple periodicities are interesting, for example, if the periodicity of the vibrating process is to be avoided. Instead of inducing a stochastic vibration, it could be enough to keep a sinusoidal vibration and tune  $\Gamma$  to the nearest red zone for your given  $\alpha$ .

Looking at the isoperiodic map of Figure 2, there is a large green zone at the top and left region of the parameter space with a single period, which continues to higher  $\alpha$  values. Zones with two and three or more flights appear periodically as one moves to the lower right corner of the map. A good rule of thumb will be to raise  $\alpha$  or lower  $\Gamma$  in order to approach a single flight zone, as it was expected. For example, when dissipation is important (large  $\alpha$ ), the single period zone becomes independent of  $\Gamma$  over a wide range (in this case

within the explored range), as was shown in a related study dealing with flight dynamics of a grain filled ball.<sup>31</sup>

As we mentioned earlier, the limit  $\alpha \rightarrow 0$  is precisely the regime when it is known that the IBBM describes the flight dynamics of granular beds in the limit of shallow and dense beds or when air is evacuated.<sup>20,25–27</sup> To give an idea of the order of magnitude of  $\alpha$ , we list in Table 1 its value or range of values for some selected previous works. We also include in Figure 3 a graphical illustration of the parameter range explored by those works. On a coarse approximation, we can see how studies where the IBBM has been reported to hold (without vacuum)<sup>20,26,27</sup> have  $\alpha < 0.2$ . Recent works on the effect of air on vibrated bed dynamics<sup>41,42,52</sup> have been done for  $0.1 < \alpha < 0.5$ . Experimental studies on the motion of vibrated beds where there is a strong and notorious effect of interstitial air have  $\alpha$  ranges that can reach 10 or more for the lowest frequencies and smaller grains. It is worth recalling an observation reported by Douady et al.<sup>25</sup> when they used water instead of air as interstitial fluid: no period bifurcation was observed for their glass spheres up to  $\Gamma = 13$ . This last configuration will imply  $\alpha \approx 30$  (without considering buoyancy and effective mass

corrections<sup>58</sup>) and represents a limiting case illustrating the large single period zone predicted for large  $\alpha$  ( $\alpha > 2$ ).

In addition, in Figure 3, we compare the results of Kroll's model with experimental data available from Han et al. The first important observation is that the qualitative agreement is remarkable. Each data set indicates a bifurcation (a periodicity change). The first bifurcation for both data sets coincides with the boundary between the first red zone and the first blue zone from the left. It is also notorious how the concavity of the boundaries (bifurcations) changes both in the theoretical map and in the experimental data. Compare the theoretical green–red boundary beginning at  $\Gamma \approx 3.1$  with a decreasing derivative with the green–red boundary beginning at  $\Gamma \approx 12.8$  with an increasing derivative. Experimental data at low  $\Gamma$  tends to lean toward right, while data sets with large  $\Gamma$  have increasing curvatures. The quantitative agreement is good for the first bifurcation and worsens for higher  $\Gamma$ . This worsening is expected because assumptions like air uncompressibility and bed behaving as a condensed block are less suited at large  $\Gamma$ .

### ■ SPECIFIC DEPENDENCE OF BED'S FLIGHT DYNAMICS ON $d$ , $\rho_g$ , $f$ , $\eta$ AND $\phi$

From a practical point of view, it may be possible to change only a single parameter at a time in order to change  $\alpha$ . Therefore, we extend our research including isoperiodic maps for all five relevant parameters entering the definition of  $\alpha$ , together with plots depicting the deviation from the IBBM with each parameter for some constant  $\Gamma$  where one period zone holds. For each case, one parameter is varied within a range spanning typical cases reported in the literature, while keeping the rest as indicated in Table 2. The particular set of parameters

**Table 2. Parameters Used To Generate the Plots at the Right Side of Figures 5, 6, 7, 8, and 9<sup>a</sup>**

parameter	symbol	value
gravity	$g$	9.8 m/s
viscosity <sup>b</sup>	$\eta$	$2 \times 10^{-5}$ Pa·s
frequency	$f$	60 Hz
porosity <sup>c</sup>	$\phi$	0.44
grain diameter	$d$	1 mm
grain density <sup>d</sup>	$\rho_g$	2500 kg/m <sup>3</sup>

<sup>a</sup>Only the parameter indicated in the horizontal axis is varied in each case. <sup>b</sup>Air at 300 K. <sup>c</sup>Experimentally measured by Sánchez et al.<sup>37</sup>

<sup>d</sup>Soda–lime glass.

in Table 3 was chosen to lay around a value of  $\alpha \approx 0.02$ , that is, below the boundary where air effects begin to be important. The influence of a change in each individual parameter is linked

**Table 3. Parameters Used To Generate the Plots of Figure 4<sup>a</sup>**

parameter	symbol	value
gravity	$g$	9.8 m/s
viscosity	$\eta$	$2 \times 10^{-5}$ Pa·s
frequency	$f$	60 Hz
porosity	$\phi$	0.36
grain diameter	$d$	0.324 mm
grain density	$\rho_g$	2500 kg/m <sup>3</sup>

<sup>a</sup>Only the parameter indicated in the horizontal axis is varied in each case.

to the corresponding change in  $\alpha$ . Therefore, we included the minimum and maximum value of  $\alpha$  for each case. Further illustration is provided in the Supporting Information, where bifurcation plots for each variable are shown (see Figure Sequences S2, S3, S4, S5, and S6). In addition and in order to give an idea of how these trends are modified when the set of parameters changes, in Figure 4 we illustrate trends for a parameter set chosen around  $\alpha \approx 0.5$  (see Table 3) where air effects are more important. It can be seen how the trends are similar, but with the case of  $\alpha \approx 0.5$  giving stronger deviations of the flight time with respect to the IBBM.

**Grain Diameter.** The sole effect of  $d$  is illustrated in Figure 5. The top left map shows an almost constant vertical structure except for low diameters, indicating how for diameters over 2 mm, the periodicity of the bed's flight dynamics is almost independent of  $d$  for the  $\Gamma$  range explored. For  $d$  lower than 2 mm (bottom left), there is a clear change of the structure of the map with  $d$ , remarked at large  $\Gamma$ . To further illustrate the role of  $d$ , we show on the right side of Figure 5 the relative flight time predicted with Kroll's model with respect to the IBBM, for low values of  $\Gamma$  (before the first bifurcation). For almost the whole  $d$  range, Kroll's prediction is the same as IBBM's. The inset shows a zoom for low  $d$ , where the deviation from the IBBM (corresponding to a value of 1) can be appreciated in more detail. For diameters around 1 mm, the difference from the IBBM is lower than 5% (for the  $\Gamma$  values considered). If  $d$  is reduced, the deviation becomes more pronounced and increases with  $\Gamma$ . The result for low  $d$  agrees with the observation of Pak et al.<sup>56</sup> where it is reported that air effects depend strongly on grain size (they explored precisely the range  $0.1 \text{ mm} \leq d \leq 2 \text{ mm}$ ); however the effect of grain size is extremely weak above a grain size of 2 mm. The effect of grain size was also noted by Akiyama et al.<sup>59</sup> where differences in the pressure distribution along vessels of different materials observed at low grain diameters diminished when the grain size was increased, and again this observation is consistent with Kroll's picture in the sense that air effects are negligible for large diameters. If the interstitial fluid is not air but water, for example, with much larger viscosity, it is possible to expect a grain size dependence of the vibrated bed dynamics for  $d > 2$  mm. Finally, Kroll's predictions are consistent with experimental results of Han et al.,<sup>42</sup> where it is shown how bifurcations occur for higher  $\Gamma$  when  $d$  is reduced.

**Grain Density.** The isolated effect of  $\rho_g$  is explored in Figure 6, for a range covering values as low as the density of expanded polystyrene up to that of lead. Both the isoperiodic map and plots at its right indicate how the effect of  $\rho_g$  is appreciated at large  $\Gamma$  and for sufficiently low densities. The work of Ze-Hui et al.<sup>27</sup> is an example of a case where a large density hinders interstitial air effects. They used stainless steel beads, with a density of  $\sim 7400 \text{ kg/m}^3$  and found that the value of  $\Gamma$  for the first bifurcation was almost independent of grain size and similar to the values predicted by the IBBM. The first row of Table 1 from the work Ze-Hui et al.<sup>27</sup> compares  $\Gamma$  for the first bifurcation for their stainless steel beads, for ceramic balls of similar size, and for the glass beads used by Douady et al.<sup>25</sup> Heavier stainless steel beads show a lower first bifurcation  $\Gamma$  than ceramic beads (at 60 Hz), and both display a lower first bifurcation  $\Gamma$  than glass beads used in ref 25 (at 30 Hz). Although the first bifurcation agrees with Kroll's prediction, it is not the same for higher bifurcations (see the rest of Table 1 from ref 27).

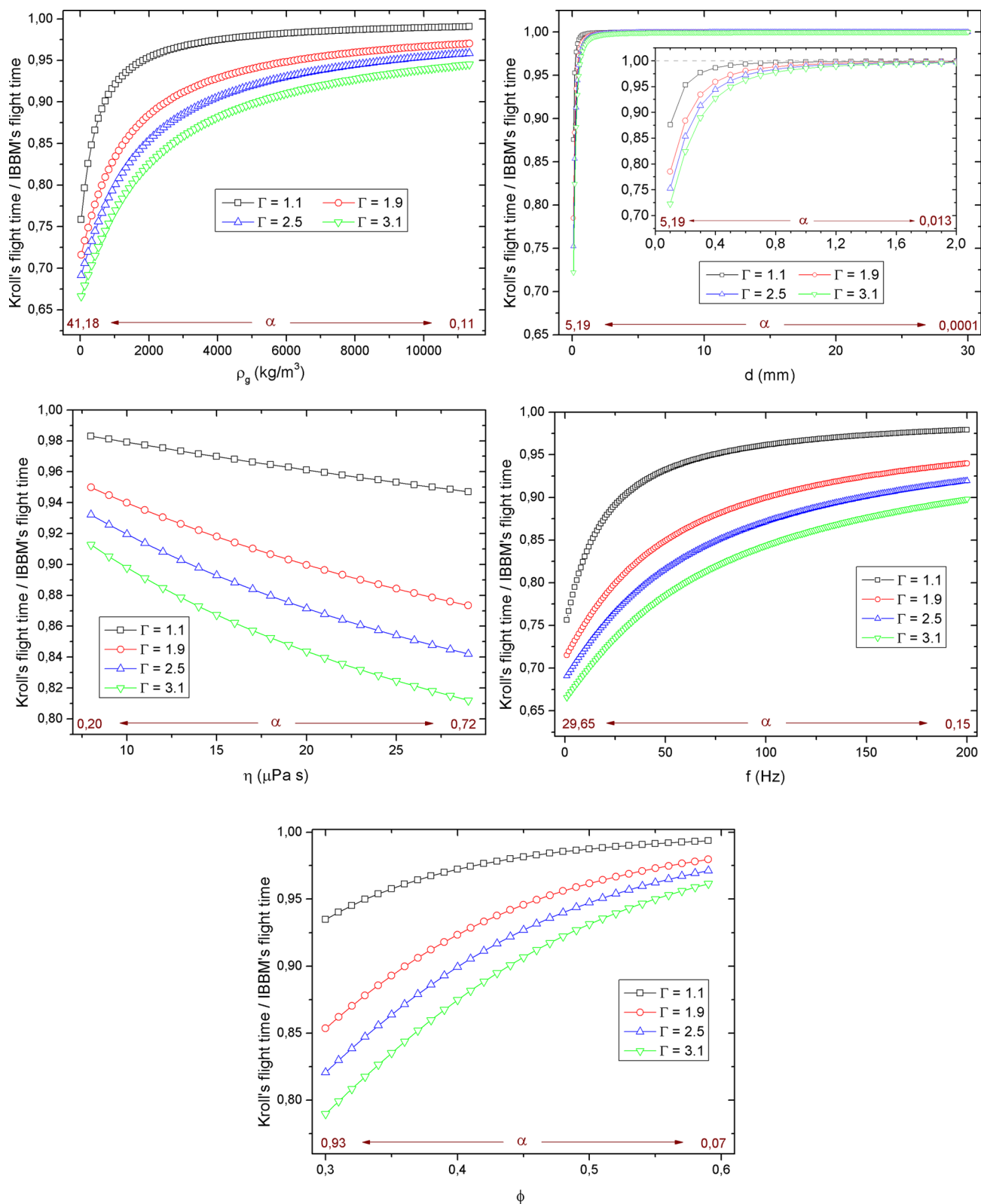


**Figure 4.** Dependence of flight time with five parameters at fixed  $\Gamma$ . Only a couple of low  $\Gamma$  cases with a single flight time are shown to illustrate the trend when the set of parameters is taken from Table 3.

**Vibration Frequency.** The isolated effect of  $f$  is explored in Figure 7. It is of special interest since  $f$  appears both in  $\alpha$  and  $\Gamma$  (the parameters controlling dissipation and forcing within the model). The map indicates how frequency affects bed dynamics specially for large  $\Gamma$ . As  $\Gamma$  decreases, the range of variability with

frequency shortens and is confined to low frequencies. The right side of Figure 7 shows how Kroll's flight time compares with that of the IBBM. Recent studies about the bifurcation pattern of vibrated beds have been done at 110 Hz<sup>41</sup> and in the 40–80 Hz range,<sup>42</sup> and even in those cases, the use of Kroll's

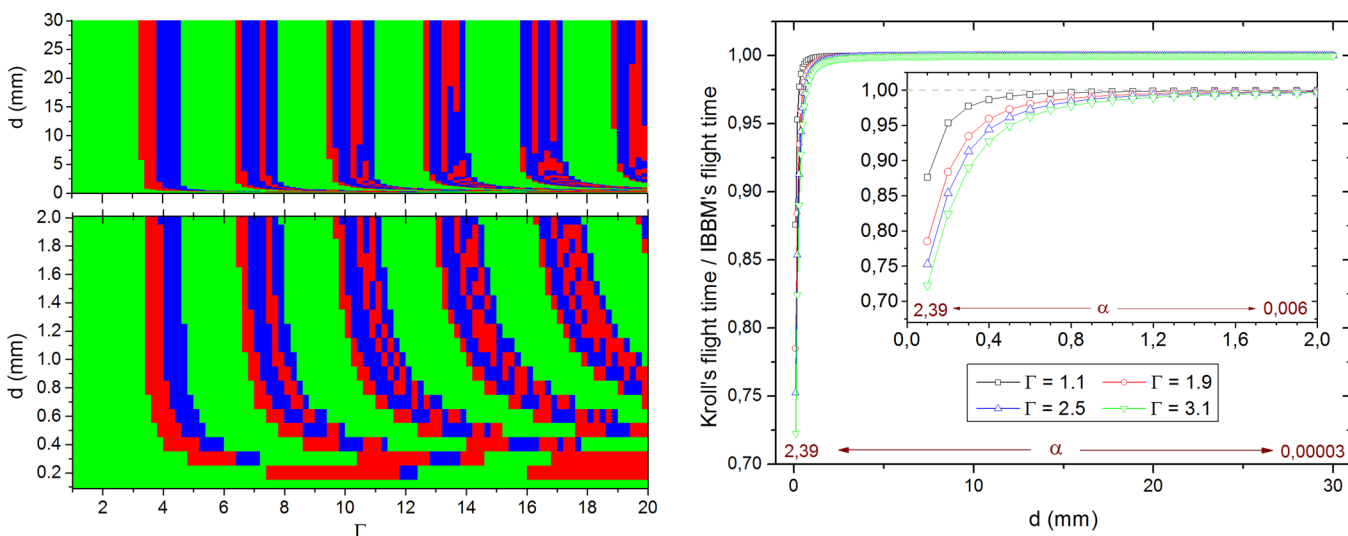


**Figure 5.** (left) Isoperiodic map  $d$ – $\Gamma$  obtained from numerical determination of the flight time of a vibrated granular bed, using Kroll's model. Green, blue, and red color indicate regions with one, two, and three or more periodic flights (see Figure 2). (right) Dependence of flight time with grain diameter  $d$  at fixed  $\Gamma$ . Only a couple of low  $\Gamma$  cases with a single flight time are shown to illustrate the trend.

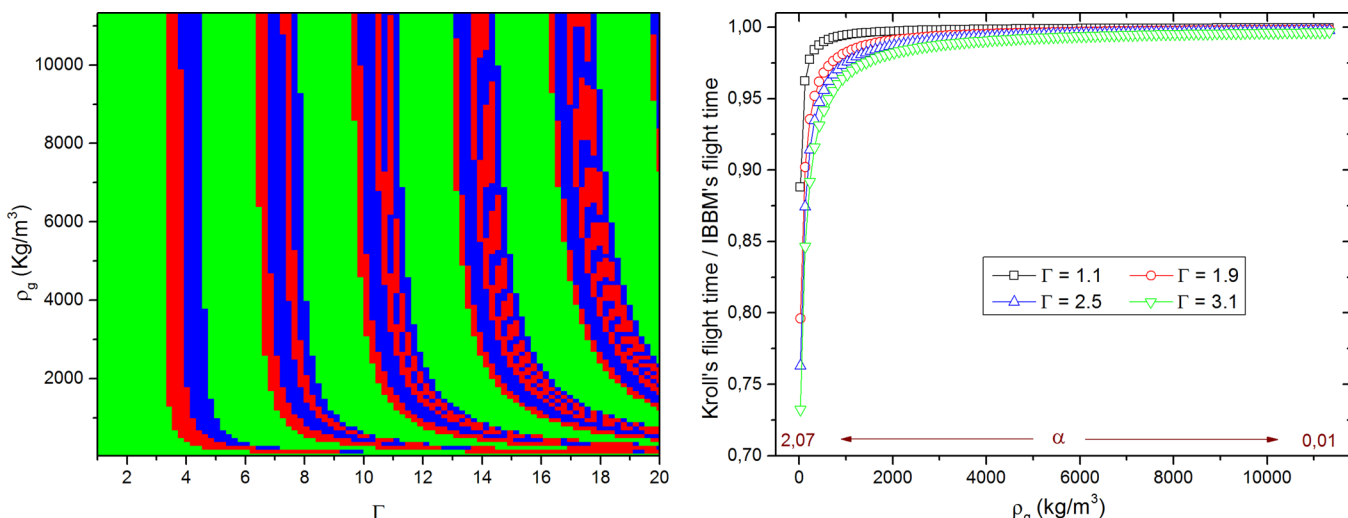


**Figure 6.** (left) Isoperiodic map  $\rho_g$ – $\Gamma$  obtained from numerical determination of the flight time of a vibrated granular bed, using Kroll's model. Green, blue, and red color indicate regions with one, two, and three or more periodic flights (see Figure 2). (right) Dependence of flight time with grain density  $\rho_g$  at fixed  $\Gamma$ . Only a couple of low  $\Gamma$  cases with a single flight time are shown to illustrate the trend.

model showed an improvement with respect to the IBBM. The improvement could have been more dramatic if lower frequencies, on the order of 10 Hz, had been used. An exception could be the work of Pastenes et al.,<sup>52</sup> whose experimental model vibrated at 15 Hz; however although their frequency was low, their granular bed was rather dense (stainless steel beads) thus reducing the value of  $\alpha$  and the relevance of air on the bed's flight dynamics. It is important to recall that many vibrated bed operations, like screening or sifting and vibratory feeding, are performed at frequencies even as low as 300 rpm (5 Hz);<sup>46,60</sup> thus studying the low frequency regime is something to be considered. Besides, many important effects of interstitial air have been reported in the low frequency regime.<sup>37,40,61–64</sup>

**Interstitial Gas Viscosity.** The isolated effect of  $\eta$  is explored in Figure 8. The range of viscosity studied corresponds to viscosities as low as that of benzene up to viscosities like that of oxygen, although rarely gases different

than air are used in the literature (an example is the work of ref 56, see Table 1). The corresponding isoperiodic map has an almost uniform vertical structure that changes marginally at large  $\Gamma$ . The relative effect of  $\eta$  is rather small when compared with the effect of  $d$  or  $f$ , and like in those cases, it is more pronounced at larger  $\Gamma$ . Figure 8, right, shows how the larger the viscosity, the larger the deviation of Kroll's model from the IBBM. Within our explored range, deviations from the IBBM do not exceed 2%.

**Bed Porosity.** The isolated effect of static bed porosity is explored in Figure 9. The range of  $\phi$  studied is rather exaggerated for a bed of monodisperse spherical particles for which the Kozeny–Karman relation (eq 3) was conceived; however it offers an idea of the role of  $\phi$ . One important concern during a vibrated bed operation may be a possible change of behavior due to compaction. We must emphasize that under Kroll's picture, the porosity is assumed as a constant during the whole vibration cycle (it is important to recall that in

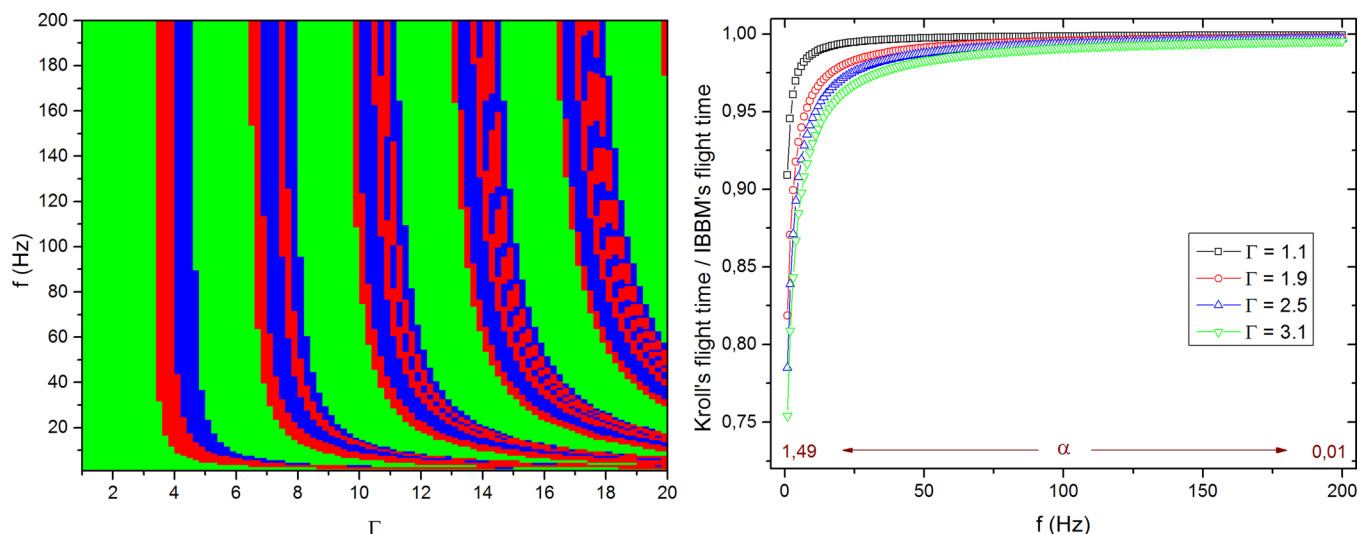


**Figure 7.** (left) Isoperiodic map  $f$ – $\Gamma$  obtained from numerical determination of the flight time of a vibrated granular bed, using Kröll's model. Green, blue, and red color indicate regions with one, two, and three or more periodic flights (see Figure 2). (right) Dependence of flight time with oscillation frequency  $f$  at fixed  $\Gamma$ . Only a couple of low  $\Gamma$  cases with a single flight time are shown to illustrate the trend.

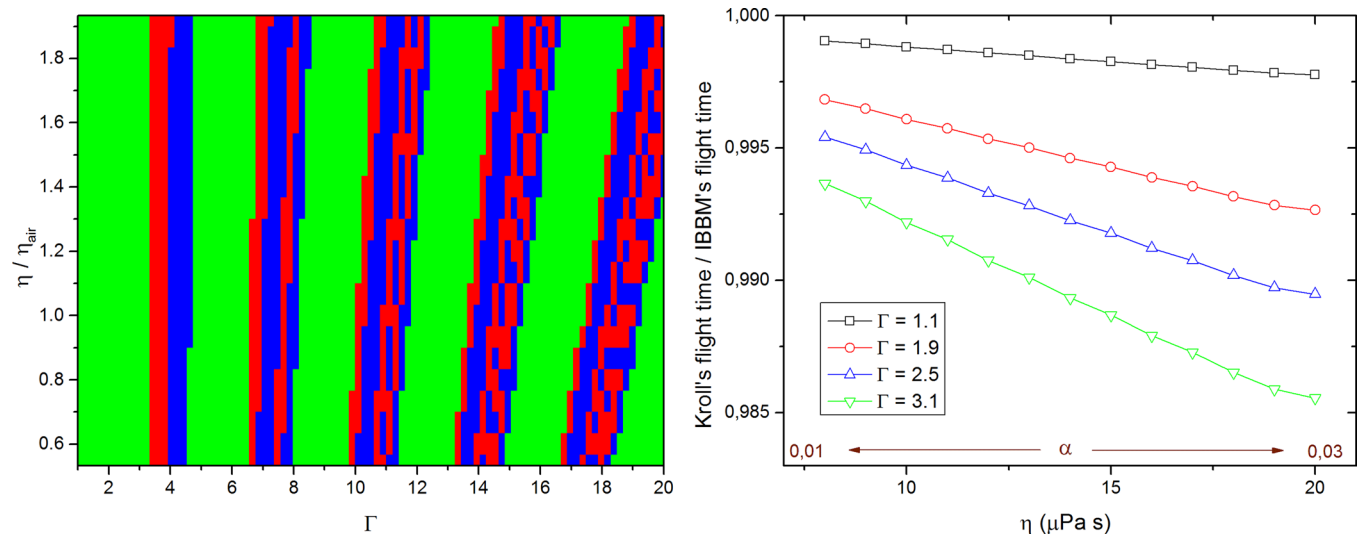


**Figure 8.** (left) Isoperiodic map  $\eta$ – $\Gamma$  obtained from numerical determination of the flight time of a vibrated granular bed, using Kröll's model. Green, blue, and red color indicate regions with one, two, and three or more periodic flights (see Figure 2). (right) Dependence of flight time with interstitial gas viscosity  $\eta$  at fixed  $\Gamma$ . Only a couple of low  $\Gamma$  cases with a single flight time are shown to illustrate the trend.

the case of vibrated shallow beds, dilation comes from the top and bottom layers, with a central bulk having almost constant density through the oscillation cycle<sup>52,65</sup>). In this section, we study variations of the static bed porosity, for example, looking at differences between a bed of elongated particles like rice grains or pellets, in contrast with a bed of spherical particles. The isoperiodic map of Figure 9 shows how the structure is almost unaffected by changes in the porosity, except for large  $\Gamma$ .

### ■ COMMENTS ON APPLICABILITY

Besides the quantitative comparison seen in Figure 3 (left), the validity of our results is founded on the validity of Kröll's model. References show how it describes the flight dynamics of a bed;<sup>41–44,52</sup> it is a good approximation for the pressure drop along a bed<sup>57</sup> and even can be applied to model transport phenomena.<sup>66</sup> The assumptions of the model are better suited for the lower left corner of all our isoperiodic maps, than for the upper right corner, where deviations due to higher speeds are

expected. However, even with a frequency of 110 Hz and  $\Gamma$  between 1 and 6, Pastor et al.<sup>41</sup> obtain fair agreement with their experimental results. If taller columns are to be considered, this analysis should have to be modified to include a proper model of the viscoelastic response of the bed as well as corrections due to spatiotemporal porosity changes. A natural next step of analysis would be to introduce the compressibility of the interstitial fluid into the picture, however in this case the solution is not as easy to obtain as in Kröll's model. Gutman<sup>67</sup> used an iterative process and Fourier series expansions, Akiyama and Naito<sup>68</sup> used the orthogonal dislocation method, and Thomas et al.<sup>57</sup> used a semiempirical method where pressure profiles were obtained from experiments and used to compute the gap height. One or several of these strategies could aid in future work; however, for the case of shallow beds, corrections should be minor.

Recent experimental investigations on the effect of interstitial air on flight dynamics of a vibrated bed<sup>41,42,52</sup> have used a

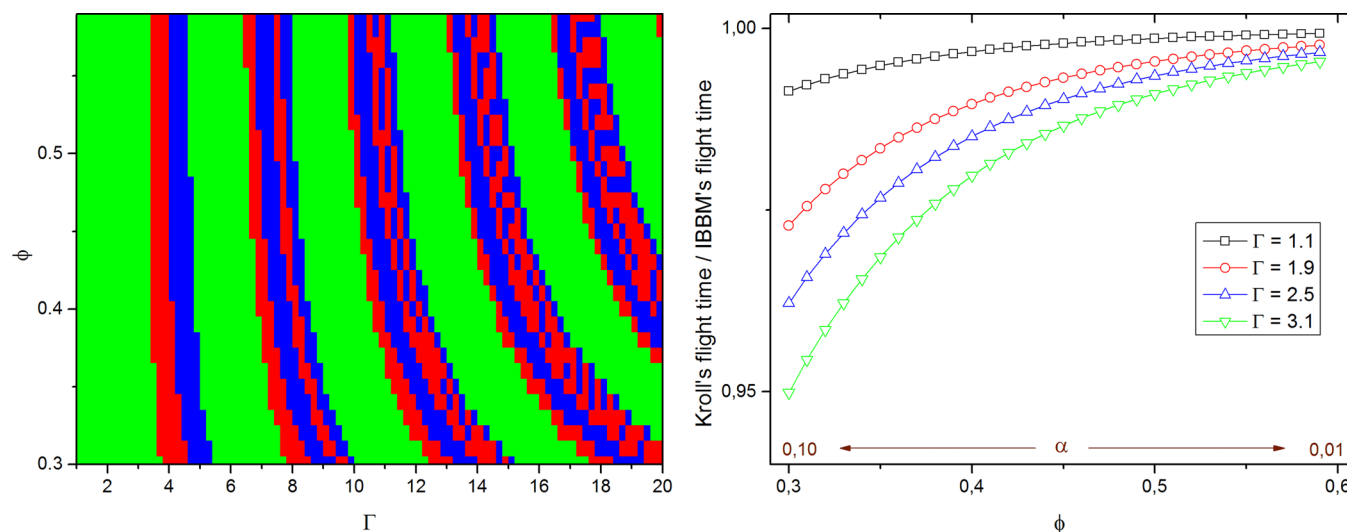


**Figure 9.** (left) Isoperiodic map  $\phi$ – $\Gamma$  obtained from numerical determination of the flight time of a vibrated granular bed, using Kroll's model. Green, blue, and red color indicate regions with one, two, and three or more periodic flights (see Figure 2). (right) Dependence of flight time with bed's porosity  $\phi$  at fixed  $\Gamma$ . Only a couple of low  $\Gamma$  cases with a single flight time are shown to illustrate the trend.

combination of parameters giving  $\alpha$  near below the limit over which air effects are dramatic (roughly 0.5). In order to further test the applicability of Kroll's model predictions, it will be interesting for future experimental explorations to perform similar studies but with a combination of parameters resulting in a larger  $\alpha$ , for example, using the frequency range of Pastenes et al.<sup>52</sup> but with glass beads of a couple hundreds of micrometers in diameter or lowering the frequency used by Pastor, Han, and their co-workers<sup>41,42</sup> to frequencies around 10 Hz.

## CONCLUSION

We have offered a discussion on modification of the flight dynamics of a shallow vibrated bed as predicted by the model of Kroll. We briefly review the model, emphasizing the fact that two parameters control bed dynamics within the model, namely, the commonly used maximum dimensionless acceleration  $\Gamma$  and a parameter  $\alpha$  defined in eq 6 quantifying dissipation due to air resistance.

We show the effects of  $\Gamma$  and  $\alpha$  on bed's flight dynamics, compared with the behavior of the inelastic bouncing ball model, where no air effects are considered. The characteristic period doubling scenario seen for the inelastic bouncing ball model is modified (specially for large  $\Gamma$ ) when  $\alpha$  is increased, reducing the number of bifurcations seen at a given  $\Gamma$  range and, in general, reducing the flight time. The plot at the right side of Figure 1 illustrates the functionality of this flight time reduction, providing an important criterion to determine the significance of interstitial air on the bed's flight dynamics.

As an alternative way to look at the dynamics of a vibrated bed, with special interest in practical industrial applications, we introduced simplified isoperiodic maps, indicating combinations of parameters that give out a single periodic motion, double period motion, or motion with more than two flight times. These maps represent an important qualitative tool to aid the design of vibrated bulk materials processing equipment or experimental protocols or to aid the decision making process when an unexpected change is to be applied to a working process. As a general rule of thumb, lowering  $\alpha$  or increasing  $\Gamma$  will drive a vibrated bed to a zone with single period motion.

The parameter  $\alpha$  depends on five quantities, namely, grain diameter  $d$ , vibration frequency  $f$ , grain density  $\rho_g$ , interstitial air viscosity  $\eta$ , and the bed's porosity  $\phi$ . By looking at deviations of Kroll's model prediction of the flight time from that of IBBM's within a typically reported range of these parameters, we can conclude that  $\phi$  and  $\eta$  do not produce important deviations, while  $d$ ,  $f$ , and  $\rho_g$  can induce deviations of the order of 25% within the range explored in this work (based on the range used by experiments reported in the literature). This deviation offers a reference frame to understand the functionality of each parameter and how they determine bed flight dynamics, information that is not evident from the equation of motion consider by Kroll's model. Combining the functionality of the deviations with the structure of isoperiodic maps, our analysis (within the context of parameters indicated in Table 2) sustains how air effects become important for grain diameters under 1 mm, frequencies under 50 Hz, and grain densities below 500 kg/m<sup>3</sup>, as have been experimentally reported before.

## ASSOCIATED CONTENT

### Supporting Information

The Supporting Information is available free of charge on the ACS Publications website at DOI: 10.1021/acs.iecr.5b04912.

Figure sequences depicting bifurcation diagrams with  $\alpha$ ,  $d$ ,  $\rho_g$ ,  $f$ ,  $\eta$ , and  $\phi$  (PDF)

## AUTHOR INFORMATION

### Corresponding Author

\*E-mail: [ijsanche@ivic.gob.ve](mailto:ijsanche@ivic.gob.ve); [isanchez@castillomax.com](mailto:isanchez@castillomax.com).

### Present Addresses

‡Departamento de Física y Matemática Aplicada, Facultad de Ciencias, Universidad de Navarra, AP 31080 Pamplona, Spain.

§Research and Development Direction, Castillomax Oil and Gas S.A., Caracas, Venezuela.

### Notes

The authors declare no competing financial interest.

## ACKNOWLEDGMENTS

We thank G. Gutiérrez, S. McNamara, J. R. Darias, C. Colonnello, and L. Reyes for fruitful discussions and S. McNamara, C. Colonnello, J. Petit, and J. Renaud for revising the manuscript. This work was funded by projects IVIC-087 and DID-USB-S1-IN-CB-004-10.

## REFERENCES

- (1) Redford, A.; Boothroyd, G. Vibratory Feeding. *Proc. - Inst. Mech. Eng.* **1967**, *182*, 135.
- (2) Takahashi, H.; Suzuki, A.; Tanaka, T. Behaviour of a Particle Bed in the Field of Vibration I. *Powder Technol.* **1968**, *2*, 65.
- (3) Suzuki, A.; Takahashi, H.; Tanaka, T. Behaviour of a Particle Bed in the Field of Vibration II. *Powder Technol.* **1968**, *2*, 72.
- (4) Kano, T. Reduction of Power Consumption in Pneumatic Conveying of Granular Materials through a Pipeline. *KONA* **1984**, *2*, 24.
- (5) Sloot, E.; Kruyt, N. Theoretical and Experimental Study of the Transport of Granular Materials by Inclined Vibratory Conveyors. *Powder Technol.* **1996**, *87*, 203.
- (6) Harada, S.; Li, H.; Funatsu, K.; Tomita, Y. Spouting of Fine Powder from Vertically Vibrated Bed. *Chem. Eng. Sci.* **2002**, *57* (5), 779.
- (7) Darias, J.; Sánchez, I.; Gutiérrez, G. Experimental Study on the Vertical Motion of Grains in a Vibrated U-tube. *Granular Matter* **2011**, *13*, 13.
- (8) Bukareva, M.; Chlenov, V.; Mikhailov, N. Drying Ferrite Powder in a Vibratory Fluidized Bed. *Powder Metallurgy and Metal Ceramics* **1967**, *6*, 664.
- (9) Majumdar, A.; Strumillo, C.; Pakowski, Z. Drying of Granular Products in Vibrofluidized Beds. In *Drying '80, Proceedings of the 2nd International Symposium on Drying, Montreal*; Mujumdar, A. S., Ed.; Hemisphere Pub. Corp.: Washington, DC, 1980; p 211.
- (10) Thomas, B.; Mason, M.; Sprung, R.; Liu, Y.; Squires, A. Heat Transfer in Shallow Vibrated Beds. *Powder Technol.* **1998**, *99*, 293.
- (11) Siebert, A.; Highgate, D.; Newborough, M. Heat Transfer Characteristics of Mechanically-Stimulated Particle Beds. *Appl. Therm. Eng.* **1999**, *19*, 37.
- (12) Tshabalala, S. N.; Squires, A. M. Effect of Axial Gas Dispersion on MTO Light-Olefin Yield: Microreactor Data. *AIChE J.* **1996**, *42*, 2941.
- (13) Quintino, D.; Malagoni, R. Cinética de Cristalização de Sacarose em Cristalizador de Leito Vibrado. *Blucher Chem. Eng. Proc.* **2015**, *2*, 1129.
- (14) Holmes, P. The Dynamics of Repeated Impacts with a Sinusoidally Vibrating Table. *Journal of Sound and Vibration* **1982**, *84*, 173.
- (15) Pieranski, P. Jumping Particle Model. Period Doubling Cascade in an Experimental System. *J. Phys. (Paris)* **1983**, *44*, 573.
- (16) Tuffillaro, N.; Mello, T.; Choi, Y.; Albano, A. Period Doubling Boundaries of a Bouncing Ball. *J. Phys. (Paris)* **1986**, *47*, 1477.
- (17) Yoshida, T.; Kousaka, Y. Mechanism of Vibratory Packing of Granular Solids. *Kagaku Kogaku* **1966**, *30*, 1019.
- (18) Kohata, T.; Gotoh, K.; Tanaka, T. Behavior of a Particle Bed in the Field of Vibration. *Kagaku Kogaku* **1967**, *31*, 55.
- (19) Brennen, C. E.; Ghosh, S.; Wassgren, C. R. Vertical Oscillation of a Bed of Granular Material. *J. Appl. Mech.* **1996**, *63*, 156.
- (20) Wassgren, C.; Brennen, C.; Hunt, M. Vertical Vibration of a Deep Bed of Granular Material in a Container. *J. Appl. Mech.* **1996**, *63*, 712.
- (21) van Doorn, E.; Behringer, R. Dilation of a Vibrated Granular Layer. *Europhys. Lett.* **1997**, *40*, 387.
- (22) Gilet, T.; Vandewalle, N.; Dorbolo, S. Completely Inelastic Ball. *Phys. Rev. E* **2009**, *79*, 055201.
- (23) Luding, S.; Clément, E.; Blumen, A.; Rajchenbach, J.; Duran, J. Studies of Columns of Beads under External Vibrations. *Phys. Rev. E: Stat. Phys., Plasmas, Fluids, Relat. Interdiscip. Top.* **1994**, *49*, 1634.
- (24) Clément, E.; Duran, J.; Rajchenbach, J. Experimental Study of Heaping in a Two-Dimensional "sand pile. *Phys. Rev. Lett.* **1992**, *69*, 1189.
- (25) Douady, S.; Fauve, S.; Laroche, C. Subharmonic Instabilities and Defects in a Granular Layer under Vertical Vibrations. *Europhys. Lett.* **1989**, *8*, 621.
- (26) Melo, F.; Umbanhowar, P.; Swinney, H. Hexagons, Kinks, and Disorder in Oscillated Granular Layers. *Phys. Rev. Lett.* **1995**, *75*, 3838.
- (27) Ze-Hui, J.; Yun-Ying, W.; Jing, W. Subharmonic Motion of Granular Particles under Vertical Vibrations. *Europhys. Lett.* **2006**, *74*, 417.
- (28) Eichwald, B.; Argentina, M.; Noblin, X.; Celestini, F. Dynamics of a Ball Bouncing on a vibrated elastic membrane. *Phys. Rev. E* **2010**, *82*, 016203.
- (29) Hubert, M.; Ludewig, F.; Dorbolo, S.; Vandewalle, N. Bouncing dynamics of a Spring. *Phys. D* **2014**, *272*, 1.
- (30) Gilet, T.; Terwagne, D.; Vandewalle, N.; Dorbolo, S. Dynamics of a Bouncing Droplet onto a Vertically Vibrated Interface. *Phys. Rev. Lett.* **2008**, *100*, 167802.
- (31) Pacheco-Vázquez, F.; Ludewig, F.; Dorbolo, S. Dynamics of a Grain-Filled Ball on a Vibrating Plate. *Phys. Rev. Lett.* **2014**, *113*, 118001.
- (32) Naylor, M.; Sánchez, P.; Swift, M. Chaotic Dynamics of an Air-Damped Bouncing Ball. *Phys. Rev. E: Stat. Phys., Plasmas, Fluids, Relat. Interdiscip. Top.* **2002**, *66*, 057201.
- (33) Han, H.; Jiang, Z.; Zhang, R.; Lyu, J. Subharmonic Bifurcations and Chaotic Dynamics of an Air Damping Completely Inelastic Bouncing Ball. *Eur. Phys. J. B* **2013**, *86*, 487.
- (34) Yan, X.; Shi, Q.; Hou, M.; Lu, K.; Chan, C. Effects of Air on the Segregation of Particles in a Shaken Granular Bed. *Phys. Rev. Lett.* **2003**, *91*, 014302.
- (35) Naylor, M.; Swift, M.; King, P. Air-Driven Brazil Nut Effect. *Phys. Rev. E: Stat. Phys., Plasmas, Fluids, Relat. Interdiscip. Top.* **2003**, *68*, 012301.
- (36) Reyes, L.; Sánchez, I.; Gutiérrez, G. Air Driven Reverse Buoyancy. *Phys. A* **2005**, *358*, 466.
- (37) Sánchez, I.; Gutiérrez, G.; Zuriguel, I.; Maza, D. Sinking of Light Intruders in a Shaken Granular Bed. *Phys. Rev. E* **2010**, *81*, 062301.
- (38) Thomas, B.; Squires, A. Support for Faraday's View of Circulation in a Fine-Powder Chladni Heap. *Phys. Rev. Lett.* **1998**, *81*, 574.
- (39) Urbina, R.; Díaz, K.; Bramer-Escamilla, W.; Sánchez, I. A Granular Fountain. *Am. J. Phys.* **2014**, *82*, 708.
- (40) Sánchez, I.; Darias, J.; Paredes, R.; Lobb, C.; Gutiérrez, G. Vertical Granular Transport in a Vibrated U-tube. *Traffic and Granular Flow'07*, Appert-Rolland, C., Chevoir, F., Gondret, P., Lassarre, S., Lebacque, J.-P., Schreckenberg, M., Eds.; Springer: Berlin, 2009; pp 545–555.
- (41) Pastor, J.; Maza, D.; Zuriguel, I.; Garcimartín, A.; Boudet, J. Time Resolved Particle Dynamics in Granular Convection. *Phys. D* **2007**, *232*, 128.
- (42) Han, H.; Jiang, Z.; Zhang, R.; Lyu, J. The Influence of Air on Period Doubling Motion in Vertically Vibrated Grains Beds. *Phys. A* **2014**, *403*, 265.
- (43) Kroll, W. Über Das Verhalten von Schüttgut in Lotrecht Schwingenden Gefäßen. *Forsch. Ingenieurwes.* **1954**, *20*, 2.
- (44) Kroll, W. Fliesserscheinungen an Haufwerken in Schwingenden Gefäßen. *Chem. Ing. Tech.* **1955**, *27*, 33.
- (45) Singh, R. Vibratory Separators Still Make the Grade for Screening Dry Bulk Powders. *Filtr. Sep.* **2004**, *41*, 20.
- (46) Masuda, H.; Higashitani, K.; Yoshida, H. *Powder Technology: Fundamentals of Particles, Powder Beds, and Particle Generation*; Taylor & Francis Group: Boca Raton, FL, 2006.
- (47) Buevich, Y.; Galontsev, V. Vibrational Fluidization of a Shallow Granular Bed. *J. Eng. Phys. (N. Y.)* **1978**, *34* (3), 259.
- (48) Erdész, K.; Halász, G. Hydrodynamic Studies of Fluidized-Beds 9. The Mechanically Analogous Model of Vibrofluidized Bed. *Hung. J. Ind. Chem.* **1984**, *12*, 441.

- (49) Bear, J. *Dynamics of Fluids in Porous Media*; Dover Publications Inc: New York, 1988.
- (50) Nedderman, R. M. *Statics and Kinematics of Granular Materials*; Cambridge University Press: Cambridge, U.K., 2005.
- (51) Rhodes, M. *Introduction to Particle Technology*, 2nd ed.; John Wiley & Sons: Hoboken, NJ, 2008.
- (52) Pastenes, J.; Géminard, J.; Melo, F. Interstitial Gas Effect on Vibrated Granular Columns. *Phys. Rev. E* **2014**, *89*, 062205.
- (53) Bagnold, R. Experiments on a Gravity-Free Dispersion of Large Solid Spheres in a Newtonian Fluid Under Shear. *Proc. R. Soc. London, Ser. A* **1954**, *225*, 49.
- (54) Miller, J.; Page, S. *Complex Adaptive Systems: An Introduction to Computational Models of Social Life*; Princeton Studies in Complexity; Princeton University Press: Princeton, NJ, 2009.
- (55) Akiyama, T.; Yamaboshi, H. Behaviour of Vibrating Beds of Irregular Particles. *Powder Technol.* **1992**, *69*, 163.
- (56) Pak, H.; van Doorn, E.; Behringer, R. Effects of Ambient Gases on Granular Materials under Vertical Vibration. *Phys. Rev. Lett.* **1995**, *74*, 4643.
- (57) Thomas, B.; Mason, M.; Squires, A. Some Behaviors of Shallow Vibrated Beds across a Wide Range in Particle Size and their Implications for Powder Classification. *Powder Technol.* **2000**, *111*, 34.
- (58) King, P.; Lopez-Alcaraz, P.; Pacheco-Martinez, H.; Clement, C.; Smith, A.; Swift, M. Instabilities in Vertically Vibrated Fluid-Grain Systems. *Eur. Phys. J. E: Soft Matter Biol. Phys.* **2007**, *22*, 219.
- (59) Akiyama, T.; Yoshikawa, T. Effects of Vessel Material on the Air Pressure Distribution within Vibrating Particle Beds. *Powder Technol.* **1999**, *103*, 139.
- (60) Schulze, D. *Powders and Bulk Solids: Behavior, Characterization, Storage and Flow*; Springer-Verlag: Berlin, 2007.
- (61) Möbius, M.; Cheng, X.; Karczmar, G.; Nagel, S.; Jaeger, H. Intruders in the Dust: Air-Driven Granular Size Separation. *Phys. Rev. Lett.* **2004**, *93*, 198001.
- (62) Caballero, L.; Melo, F. Droplets of Fine Powders Running Uphill by Vertical Vibration. *Phys. Rev. Lett.* **2004**, *93*, 258001.
- (63) van Gerner, H.; van der Hoef, M.; van der Meer, D.; van der Weele, K. Interplay of Air and Sand: Faraday Heaping Unravelling. *Phys. Rev. E* **2007**, *76*, 051305.
- (64) Liu, C.; Wu, P.; Zhang, F.; Wang, L. Particle Climbing Induced by Reciprocating Air Flow. *Appl. Phys. Lett.* **2013**, *102*, 183507.
- (65) Idler, V.; Sánchez, I.; Paredes, R.; Gutiérrez, G.; Reyes, L. I.; Botet, R. Three-Dimensional Simulations of a Vertically Vibrated Granular Bed Including Interstitial Air. *Phys. Rev. E* **2009**, *79*, 051301.
- (66) Clement, C.; Pacheco-Martinez, H.; Swift, M.; King, P. Partition Instability in Water-Immersed Granular Systems. *Phys. Rev. E* **2009**, *80*, 011311.
- (67) Gutman, R. Vibrated Bed of Particles: A Simple Model for the Vibrated Bed. *Trans. Inst. Chem. Eng.* **1976**, *54*, 174.
- (68) Akiyama, T.; Naito, T. Vibrated Bed of Powders: A New Mathematical Formulation. *Chem. Eng. Sci.* **1987**, *42*, 1305.